

Electric Supplemental Information for:

Structure and Bifunctional Electrocatalytic Activity of A Novel 3D Framework Based on Dimeric Monocupper-Substituted Polyoxoanions as Ten-connected linkages †

Shaobin Li, Wei Zhu, Huiyuan Ma*, Haijun Pang*, Heng Liu and Tingting Yu

Table of contents:

1. **Table S1** Summarization of known hybrids based type II dimers.
2. **Table S2** Selected bond lengths [\AA] and bond angles [°] for compound **1**.
3. **Fig. S1** Schematic view of $[\text{Cu}(\text{en})_2]^{2+}$ complex as a 2-connected node and $(\text{PW}_{11}\text{Cu})_2$ dimer as a 10-connected node.
4. **Chart S1** Structures of dap and en molecules.
5. **Fig. S2** The IR spectrum of **1**
6. **Fig. S3** The simulative (black) and experimental (red) PXRD patterns of compound **1**.
7. **Fig. S4** TG curve of compound **1**
8. **Fig. S5** Cyclic voltammogram of **1**-CPE
9. **Fig. S6** Oxidation of AA and DA at **1**-CPE in HAc-NaAc buffer solution in the potential range of 0.0 – 0.7 V.

Table S1 Summarization of known hybrids based type II dimers

Compounds	Connection number of the dimers	Dimension of structures	References
$[\{\gamma\text{-SiTi}_2\text{W}_{10}\text{O}_{36}(\text{OH})_2\}_2(\mu\text{-O})_2]^{8-}$	0	0D	24d
$[\{\gamma\text{-SiTi}_2\text{W}_{10}\text{O}_{36}(\text{OMe})_2\}_2(\mu\text{-O})_2]^{8-}$	0	0D	24d
A- α - $[(\text{SiNb}_3\text{W}_9\text{O}_{38})_2(\mu\text{-O})_2]^{10-}$	0	0D	24e
$[\text{Cu}(\text{dap})_2]_2\{[\text{Cu}(\text{dap})_2]_2[\text{Cu}(\text{dap})_2][\text{PCuW}_{11}\text{O}_{39}]_2\}$	4	1 D	24f

Table S2. The selected bond lengths (\AA) and angles (deg) for **1**.

W(1)-O(21)	1.707(16)	W(4)-O(14)	1.721(18)
W(1)-O(23)	1.837(16)	W(4)-O(13)	1.78(2)
W(1)-O(20)	1.908(16)	W(4)-O(11)	1.857(15)
W(1)-O(22)	1.960(14)	W(4)-O(16)	1.929(18)
W(1)-O(18)	2.013(16)	W(5)-O(17)	1.70(2)
W(2)-O(9)	1.706(14)	W(5)-O(18)	1.894(19)
W(2)-O(2)	1.828(15)	W(6)-O(10)	1.68(3)
W(2)-O(20)	1.906(16)	W(6)-O(8)	1.828(13)
W(2)-O(7)	1.914(18)	W(6)-O(13)	1.95(2)
W(2)-O(11)	2.006(16)	W(6)-O(12)	2.43(2)
W(2)-O(26)	2.300(14)	W(7)-O(1)	1.844(5)
W(3)-O(5)	1.709(17)	W(7)-O(4)	1.929(8)
W(3)-O(4)	1.851(17)	W(7)-O(23)	1.942(16)
W(3)-O(6)	1.891(5)	W(7)-O(3)	1.948(17)
O(21)-W(1)-O(23)	101.8(8)	O(20)-W(1)-O(19)	85.1(6)
O(21)-W(1)-O(20)	103.1(8)	O(22)-W(1)-O(19)	73.4(8)
O(23)-W(1)-O(20)	91.5(7)	O(9)-W(2)-O(2)	101.8(8)
O(21)-W(1)-O(22)	97.4(9)	O(9)-W(2)-O(20)	101.7(8)
O(23)-W(1)-O(22)	91.3(8)	O(2)-W(2)-O(20)	90.0(7)
O(20)-W(1)-O(22)	158.3(8)	O(9)-W(2)-O(7)	101.0(8)
O(21)-W(1)-O(18)	96.9(9)	O(2)-W(2)-O(7)	89.1(7)
O(23)-W(1)-O(18)	161.1(8)	O(20)-W(2)-O(7)	157.0(7)
O(20)-W(1)-O(18)	86.2(7)	O(9)-W(2)-O(11)	96.6(7)
O(22)-W(1)-O(18)	84.1(8)	O(2)-W(2)-O(11)	161.6(6)
O(21)-W(1)-O(19)	165.6(8)	O(20)-W(2)-O(11)	85.2(6)
O(23)-W(1)-O(19)	89.5(7)	O(7)-W(2)-O(11)	88.4(7)

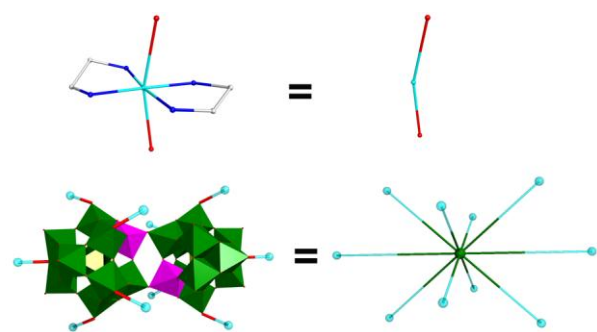


Fig. S1. Schematic view of $[\text{Cu}(\text{en})_2]^{2+}$ complex as a 2-connected node and $(\text{PW}_{11}\text{Cu})_2$ dimer as a 10-connected node.

Chart S1. Structures of dap and en molecules.

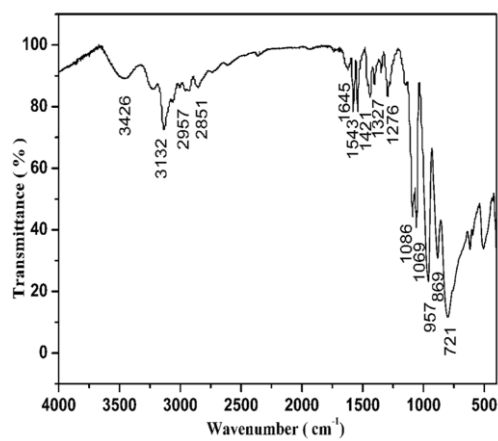
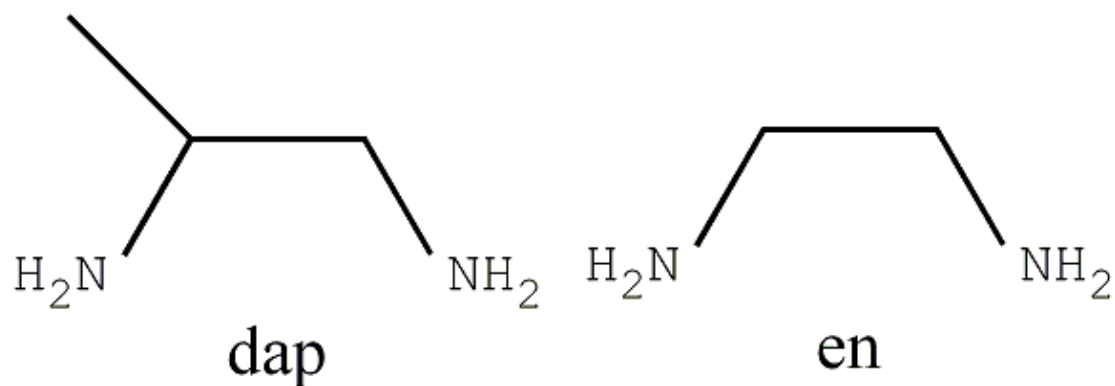


Fig. S2. The IR spectrum of **1**.

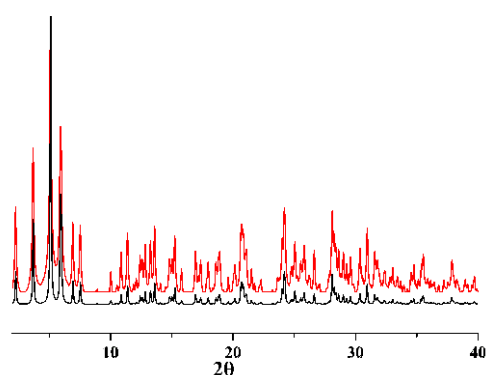


Fig. S3. The simulative (black) and experimental (red) powder X-ray diffraction patterns for **1**.

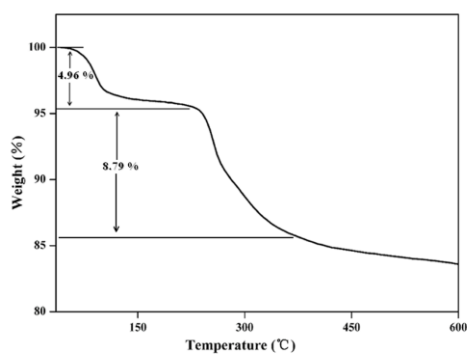


Fig. S4. The TG curve of **1**.

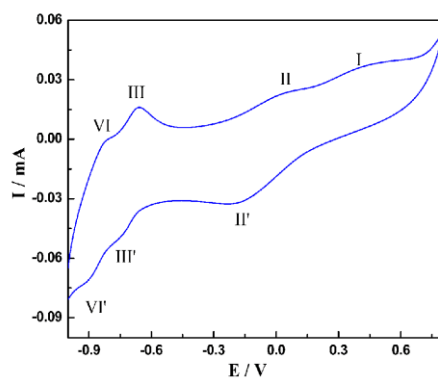


Fig. S5. Cyclic voltammogram for **1**-CPE in 0.2 M HAc-NaAc (pH=4.5) buffer solution at the scan rate of $50 \text{ mV}\cdot\text{s}^{-1}$.

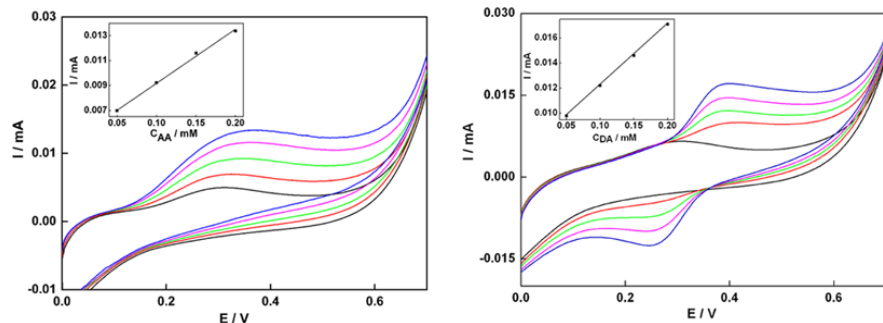


Fig. S6 Oxidation of AA (left) and DA (right) at 1-CPE in HAc-NaAc buffer solution containing AA and DA in various concentrations (from inner to outer): 0.05, 0.10, 0.15, 0.20 mM. Scan rate: $0.05 \text{ V}\cdot\text{s}^{-1}$. The inset shows a linear dependence of the anodic catalytic current of wave I with AA and DA concentration.